

Supporting Information for

Metalloporphyrin-modified semiconductors for solar fuel production

Diana Khusnutdinova, Anna M. Beiler, Brian L. Wadsworth, Samuel I. Jacob and Gary F. Moore*

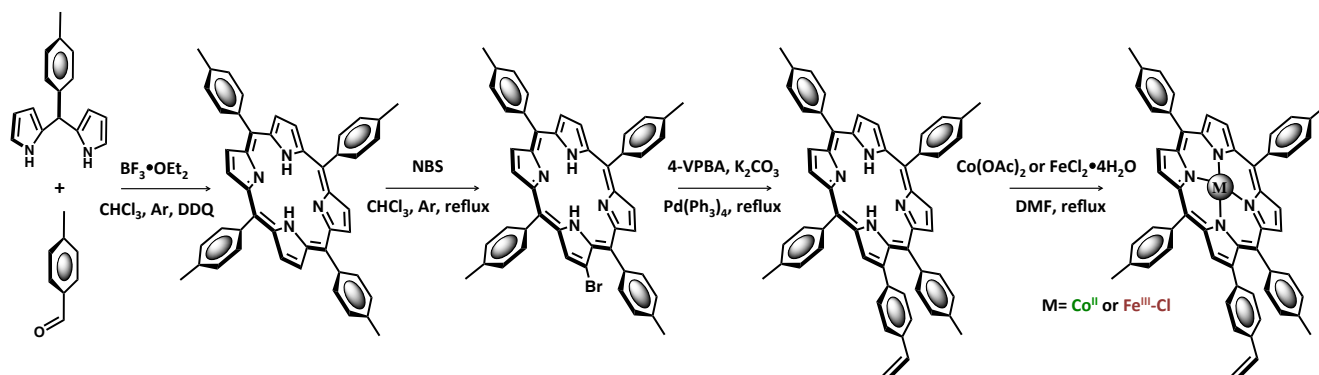
School of Molecular Sciences and the Biodesign Institute Center for Applied Structural Discovery (CASD),
Arizona State University, Tempe, AZ 85287-1604, United States
gfmoore@asu.edu

Index

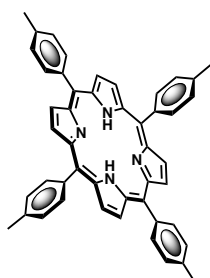
1. Molecular synthesis and characterization	S2-S12
1.1 NMR spectra	S5-S7
1.2 UV-Vis spectra	S7-S8
1.3 FTIR data	S9-S10
1.4 Electrochemical data	S11-S12
2. Surface characterization	S13-S18
2.1 FTIR data	S14-S15
2.2 XPS data	S16-S18
3. Photoelectrochemical data	S19-S22
3.1 Spectral profile of a LSC-100 Series Oriel Solar Simulator	S22
4. Supplemental information references	S23

1. Molecular synthesis and characterization

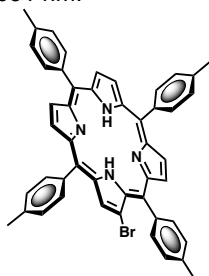
All reagents and solvents were purchased from Aldrich. Dichloromethane, hexanes, toluene and *p*-tolyl aldehyde were freshly distilled before use. Milli-Q water (18.2 MΩ cm) was used to prepare all aqueous solutions.



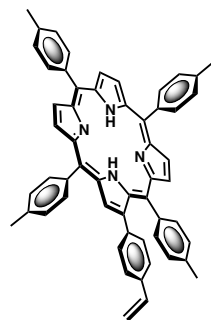
SCHEME S1. Synthetic Scheme Used to Prepare the Modified Metalloporphyrins.



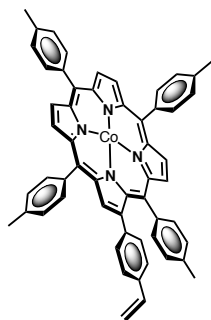
5,10,15,20-tetra *p*-tolylporphyrin. A similar method was previously reported.¹ A solution of 5-(4-methylphenyl)dipyrromethane (880 mg, 6 mmol) and *p*-tolyl aldehyde (890 mL, 6 mmol) in chloroform (600 mL) was purged for 15 min with argon before adding BF₃(OEt)₂ (33 mL of 2.5 M stock solution in chloroform, 3.3 mM). After stirring for 12 h, 2,3-dichloro-5,6-dicyano-1,4-benzoquinone (DDQ) (2.04 g, 9 mmol) was added and the mixture was stirred for an additional 3 h before adding 7.5 mL of triethylamine. The mixture was filtered through an alumina pad and the solvent was evaporated at reduced pressure. The crude product was purified by column chromatography on silica using a mixture of 2:1 chloroform and hexanes as the eluent to yield the desired product (45%). ¹H NMR (400 MHz, CDCl₃): δ -2.77 (2H, s, NH), 2.70 (12H, s, CH₃), 7.55 (8H, d, *J* = 7.8 Hz, ArH), 8.09 (8H, d, *J* = 7.8 Hz, ArH) 8.85 (8H, s, βH); MALDI-TOF-MS *m/z*. calcd. for C₄₈H₃₈N₄ 670.31, obsd. 670.46; UV-Vis (Toluene) 420, 516, 550, 593, 651 nm.



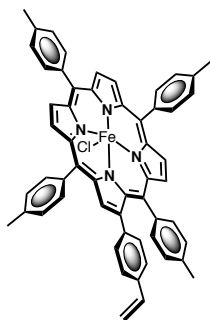
β-bromo-5,10,15,20-tetra-*p*-tolylporphyrin. A similar method was previously reported.² 5,10,15,20-tetra-*p*-tolylporphyrin (120 mg, 0.179 mmol) and pyridine (2 mL) were dissolved in chloroform (120 mL) and the solution was stirred and heated to reflux. After 15 min, a solution of *N*-bromosuccinamide (64 mg, 0.358 mmol, dissolved in 30 mL chloroform) was added dropwise over 45 min to the refluxing mixture. The reaction mixture was quenched with acetone (20 mL), and the solvent evaporated at reduced pressure. The crude residue was purified by column chromatography on silica using a mixture of 1:1 cyclohexane and chloroform as the eluent to give the desired product (45%). ¹H NMR (400 MHz, CDCl₃): δ -2.85 (2H, s, NH), 2.70 (12H, s, CH₃), 7.58-7.50 (8H, m, ArH), 7.95 (2H, d, *J* = 7.8 Hz, ArH), 8.10 (2H, d, *J* = 7.8 Hz, ArH) 8.10 (2H, d, *J* = 7.5 Hz, ArH), 8.10 (2H, d, *J* = 7.3 Hz, ArH), 8.93-8.74 (7H, m, βH); MALDI-TOF-MS *m/z*. calcd. for C₄₈H₃₇BrN₄ 748.22 (750.22), obsd. 750.64 (748.65); UV-Vis (Toluene) 422, 519, 554, 595, 651 nm.



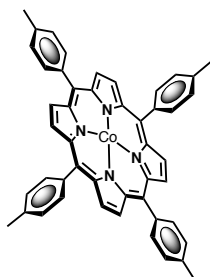
5,10,15,20-tetra-*p*-tolyl-2-(4-vinylphenyl)porphyrin. 4-vinylphenylboronic acid (4-VPBA) (89 mg, 0.6 mmol), potassium carbonate (138 mg, 1.2 mmol) and tetrakis(triphenylphosphine)palladium(0) (16 mg, 0.012 mmol) were added to a solution containing β -bromo-5,10,15,20-tetra-*p*-tolylporphyrin (90 mg, 0.12 mmol) dissolved in toluene (35 mL) and under an argon atmosphere. The reaction mixture was heated to reflux and the progress of the reaction was monitored via TLC. The reaction was stopped following consumption of the porphyrin starting material (~3-5 h) and the mixture was washed with a saturated solution of aqueous sodium bicarbonate then a saturated solution of aqueous sodium chloride. The organic phase was dried over sodium sulfate, filtered, and the solvent evaporated at reduced pressure. The residue was purified by column chromatography on silica using a mixture of 1:1 dichloromethane and hexanes as the eluent to yield the desired product (68%). $^1\text{H NMR}$ (400 MHz, CDCl_3) δ -2.63 (2H, s, NH), 2.38 (3H, s, CH_3), 2.67 (3H, s, CH_3), 2.70 (6H, s, CH_3), 5.25 (1H, d, $J = 11.1$ Hz, CH), 5.78 (1H, d, $J = 17.7$ Hz, CH), 6.76 (1H, dd, $J = 17.6$ Hz, $J = 10.87$ Hz, CH), 7.01 (2H, d, $J = 7.7$ Hz, ArH), 7.18 (2H, d, $J = 8.1$ Hz, ArH), 7.25 (2H, d, $J = 7.9$ Hz, ArH), 7.51 (2H, d, $J = 7.8$ Hz, ArH), 7.54 (2H, d, $J = 7.6$ Hz, ArH), 7.56 (2H, d, $J = 7.6$ Hz, ArH), 7.73 (2H, d, $J = 7.9$ Hz, ArH), 8.09 (2H, d, $J = 7.8$ Hz, ArH), 8.10 (2H, d, $J = 7.8$ Hz, ArH), 8.10 (2H, d, $J = 7.8$ Hz, ArH), 8.87-8.74 (7H, m, βH); MALDI-TOF-MS m/z . calcd. for $\text{C}_{56}\text{H}_{44}\text{N}_4$ 772.36, obsd. 772.42. UV-Vis (Toluene) 424, 520, 554, 597, 653 nm.



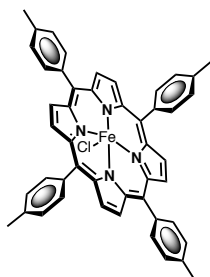
5,10,15,20-tetra-*p*-tolyl-2-(4-vinylphenyl)porphyrin cobalt(II). A mixture containing 5,10,15,20-tetra-*p*-tolyl-2-(4-vinylphenyl)porphyrin (23 mg, 0.03 mmol) and cobalt (II) acetate (53 mg, 0.3 mmol) in dimethylformamide (35 mL) was stirred at reflux for 20 min. Upon cooling, the solvent was removed at reduced pressure. The residue was purified by column chromatography on alumina using dichloromethane as eluent. Recrystallization from dichloromethane/methanol gave the target compound (98%). UV-Vis (Toluene) 421, 535 nm; MALDI-TOF-MS m/z . calcd. for $\text{C}_{56}\text{H}_{42}\text{CoN}_4$ 829.27, obsd. 829.15.



5,10,15,20-tetra-*p*-tolyl-2-(4-vinylphenyl)porphyrin iron(III) chloride. 5,10,15,20-tetra-*p*-tolyl-2-(4-vinylphenyl)porphyrin (32 mg, 0.04 mmol) was dissolved in dimethylformamide (18 mL) and the mixture was stirred and heated to reflux. Upon reaching reflux, $\text{FeCl}_2 \cdot 4\text{H}_2\text{O}$ (49 mg, 0.25 mmol) was added to the solution in three approximately equivalent portions over 30 min. Upon cooling, the solvent was evaporated at reduced pressure and the brown residue was purified on alumina column using dichloromethane as eluent. The green colored fractions obtained from chromatography were concentrated and washed with an aqueous 6M HCl solution. The organic solvent was removed under reduced pressure and the brown residue was recrystallized from methanol to give the target compound (98%). UV-Vis (Toluene) 423, 513, 578, 668, 699 nm; MALDI-TOF-MS *m/z*. calcd. for $\text{C}_{56}\text{H}_{42}\text{ClFeN}_4$ 861.24, obsd. 863.18.

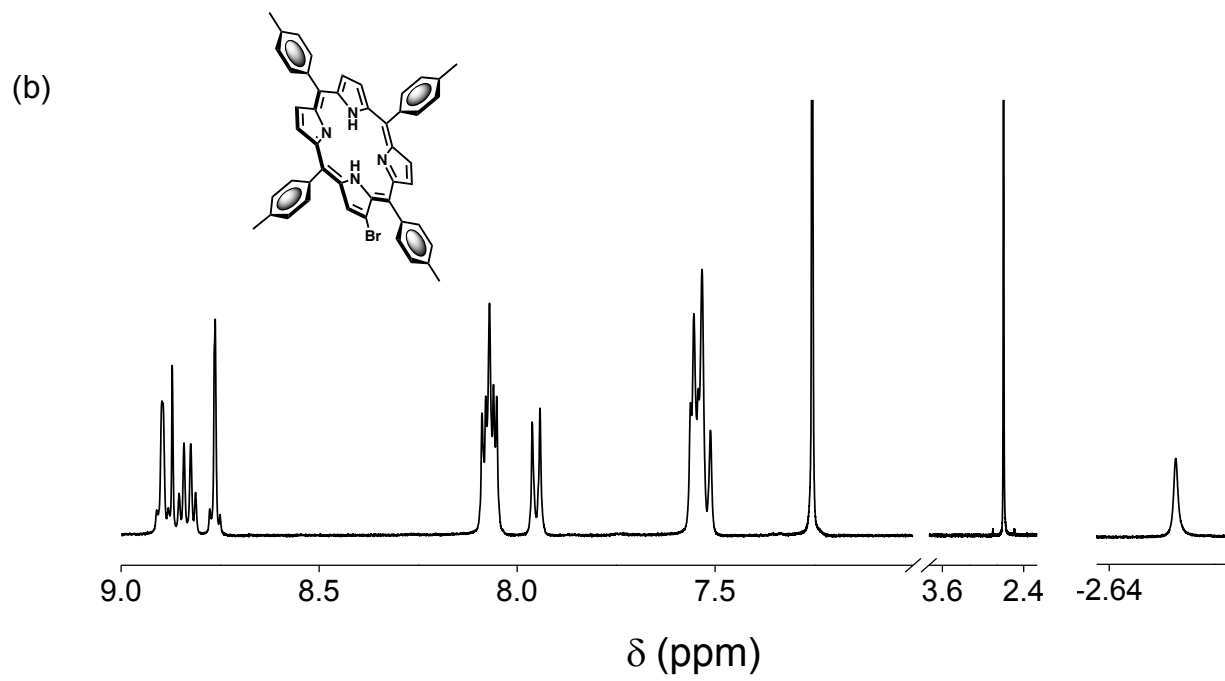
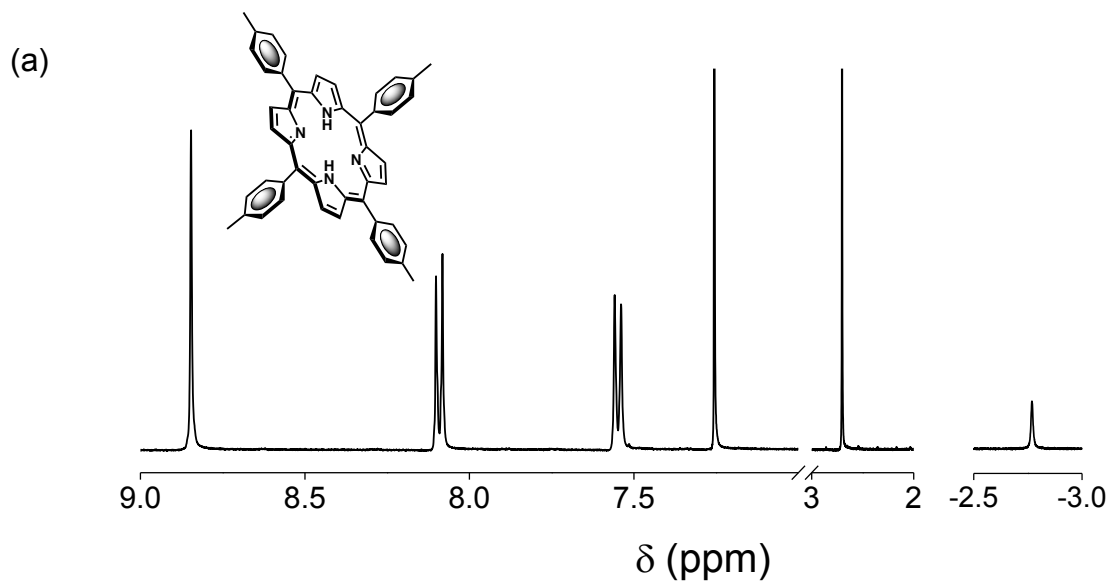


5,10,15,20-tetra-*p*-tolylporphyrin cobalt(II) (CoTTP). A similar method was previously reported.³ 5,10,15,20-tetra-*p*-tolylporphyrin (25 mg, 0.03 mmol) and a solution of cobalt (II) acetate (53 mg, 0.3 mmol) were dissolved in dimethylformamide (35 mL) and brought to reflux. The mixture was refluxed for 20 min before evaporating the solvent at reduced pressure. The product was purified on an alumina column using dichloromethane as eluent and recrystallized from dichloromethane/methanol to give a desired product (98%). UV-Vis (Toluene) 416, 530 nm.



5,10,15,20-tetra-*p*-tolylporphyrin iron(III) chloride (FeTTP). A similar method was previously reported.⁴ 5,10,15,20-tetra-*p*-tolylporphyrin (35 mg, 0.04 mmol) was dissolved in dimethylformamide (18 mL) and the mixture was stirred and heated to reflux. Upon reaching reflux, $\text{FeCl}_2 \cdot 4\text{H}_2\text{O}$ (49 mg, 0.25 mmol) was added to the solution in approximately three equivalent portions over 30 min. Upon cooling, the solvent was evaporated at reduced pressure and the brown residue was purified on an alumina column using dichloromethane as eluent. The green colored fractions obtained from chromatography were concentrated and washed with an aqueous 6M HCl solution. The organic solvent was removed under reduced pressure and the brown residue was recrystallized from methanol to give the target compound (98%). UV-Vis (Toluene) 421, 509, 571, 668, 691 nm.

1.1 NMR spectra



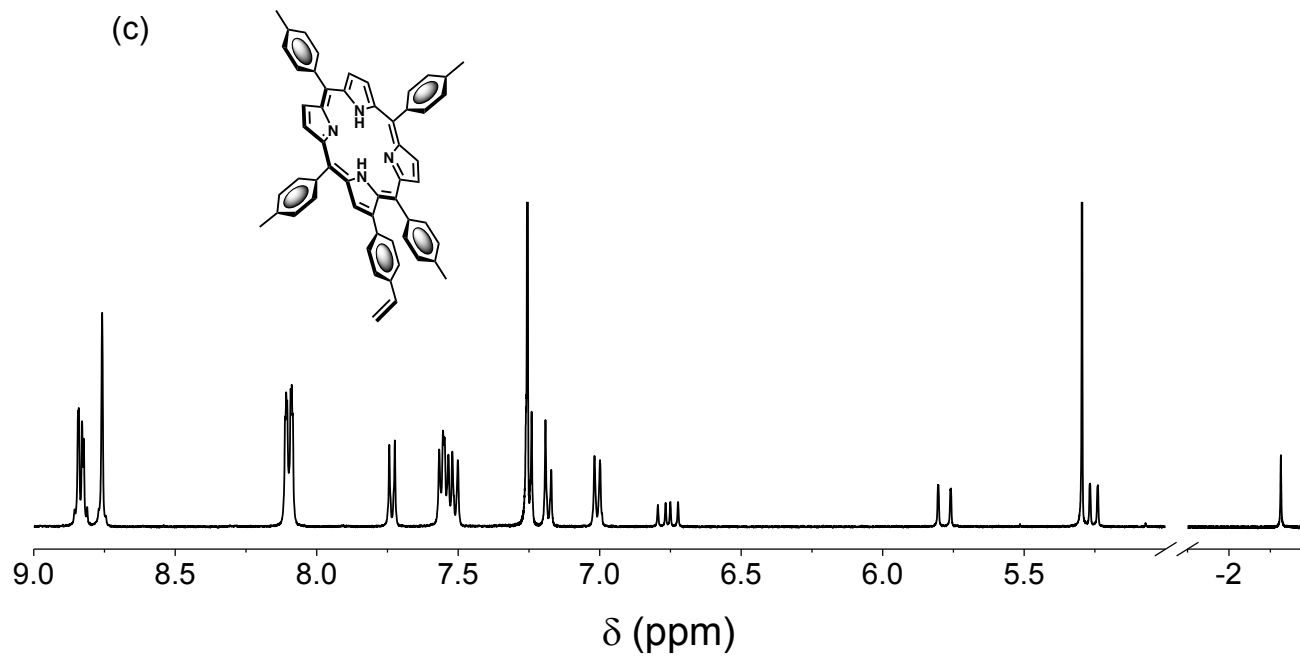


Figure S1. ^1H NMR spectra of (a) 5,10,15,20-tetra-*p*-tolylporphyrin, (b) β -bromo-5,10,15,20-tetra-*p*-tolylporphyrin, and (c) 5,10,15,20-tetra-*p*-tolyl-2-(4-vinylphenyl)porphyrin in chloroform-*d*.

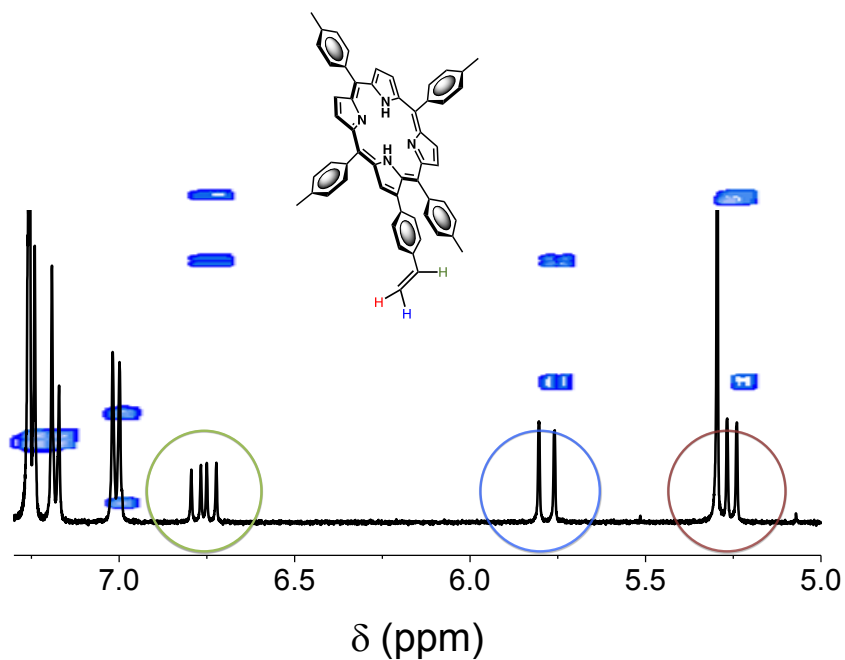


Figure S2. ^1H NMR spectra (black) with overlaid COSY (blue) of 5,10,15,20-tetra-*p*-tolyl-2-(4-vinylphenyl)porphyrin in chloroform-*d*.

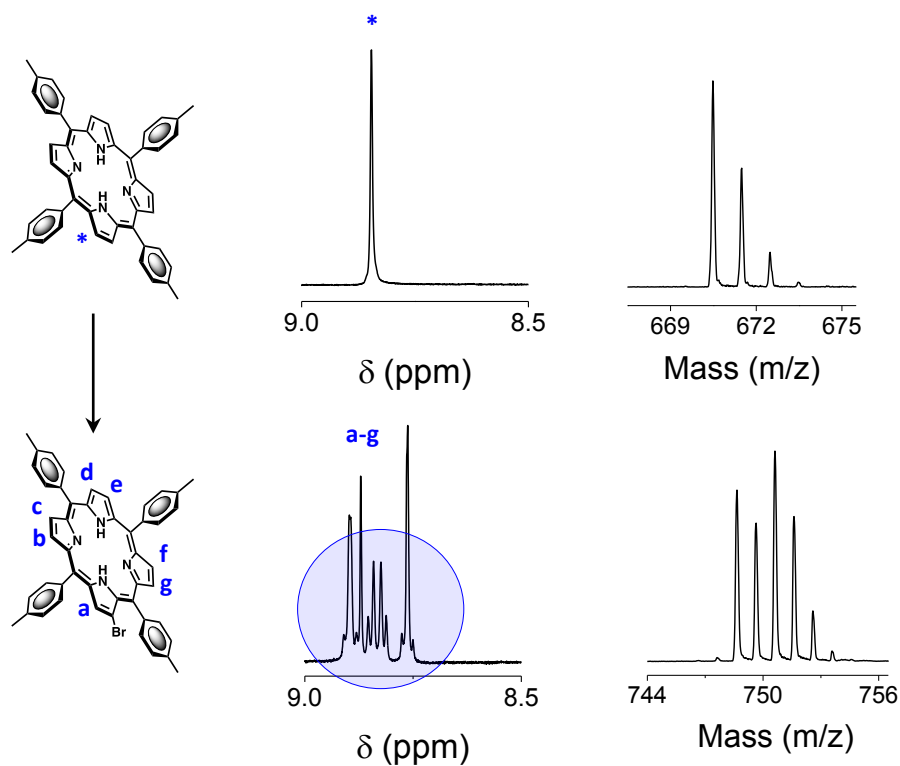


Figure S3. (left) ^1H NMR spectra showing the symmetry of the β -pyrrolic protons and (right) MALDI-TOF-MS data showing the isotopic distribution patterns of (top) 5,10,15,20-tetra-*p*-tolylporphyrin and (bottom) β -bromo-5,10,15,20-tetra-*p*-tolylporphyrin.

1.2 UV-Vis spectra

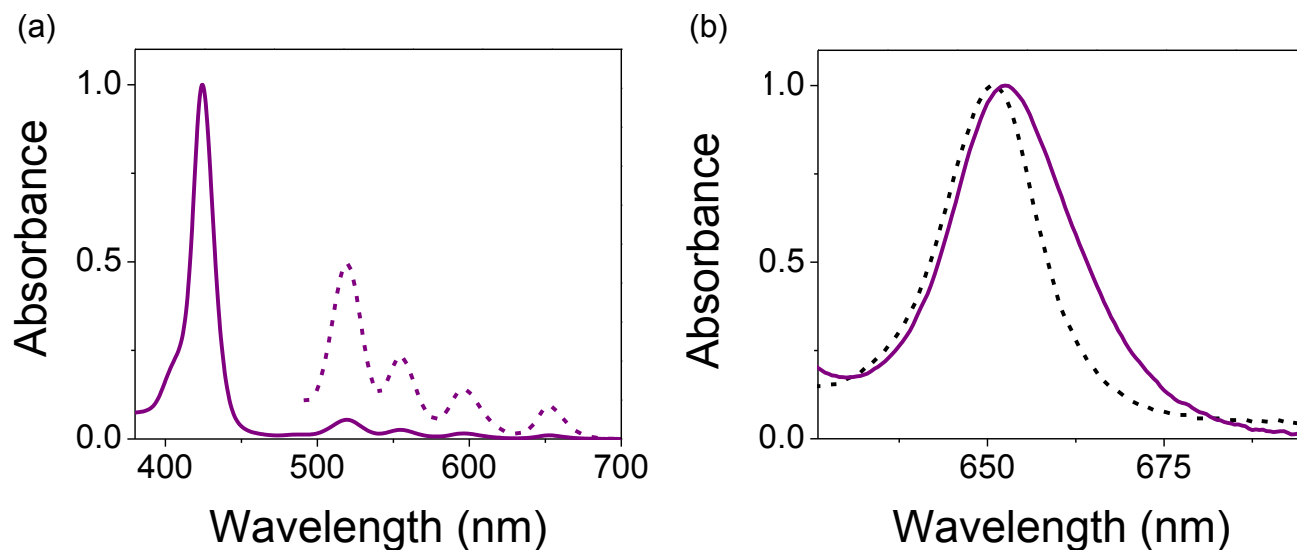


Figure S4. (a) Absorbance spectra of 5,10,15,20-tetra-*p*-tolyl-2-(4-vinylphenyl)porphyrin recorded in toluene showing the Soret band normalized to 1 (solid) and the highest energy Q band normalized to 0.5 (dashed). (b) Normalized absorbance spectra showing the lowest energy Q bands of the model compound 5,10,15,20-tetra-*p*-tolylporphyrin (dashed) and 5,10,15,20-tetra-*p*-tolyl-2-(4-vinylphenyl)porphyrin (solid) are included for comparison.

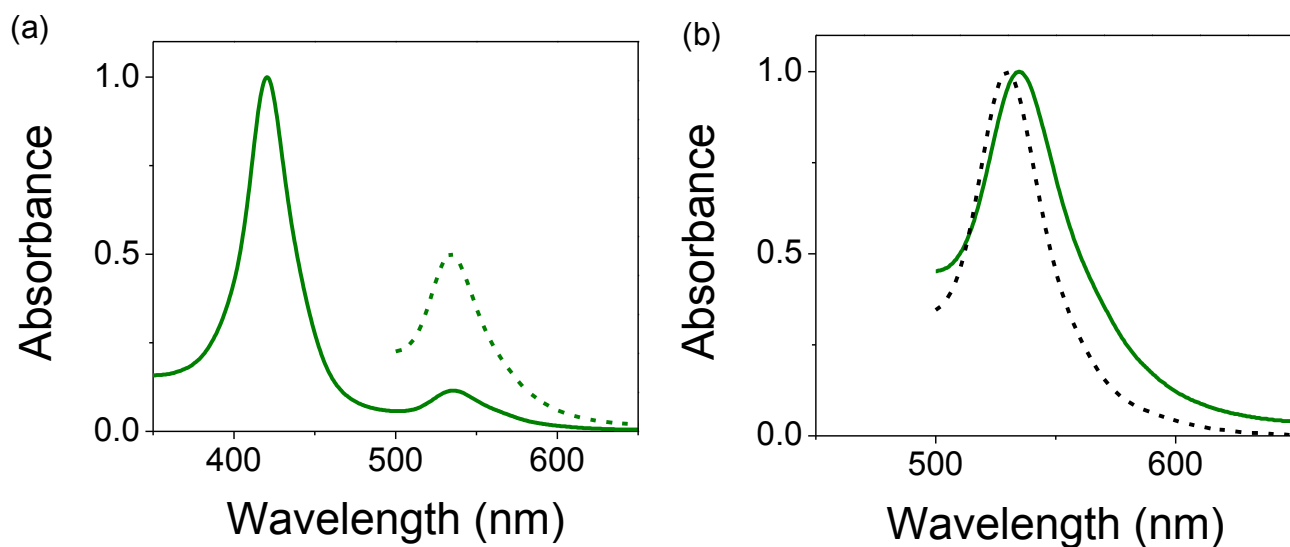


Figure S5. (a) Absorbance spectra of 5,10,15,20-tetra-*p*-tolyl-2-(4-vinylphenyl)porphyrin cobalt(II) recorded in toluene showing the Soret band normalized to 1 (solid) and the highest energy Q band normalized to 0.5 (dashed). (b) Normalized absorbance spectra showing the lowest energy Q bands of the model compound 5,10,15,20-tetra-*p*-tolylporphyrin cobalt(II) (dashed) and 5,10,15,20-tetra-*p*-tolyl-2-(4-vinylphenyl)porphyrin cobalt(II) (solid) are included for comparison.

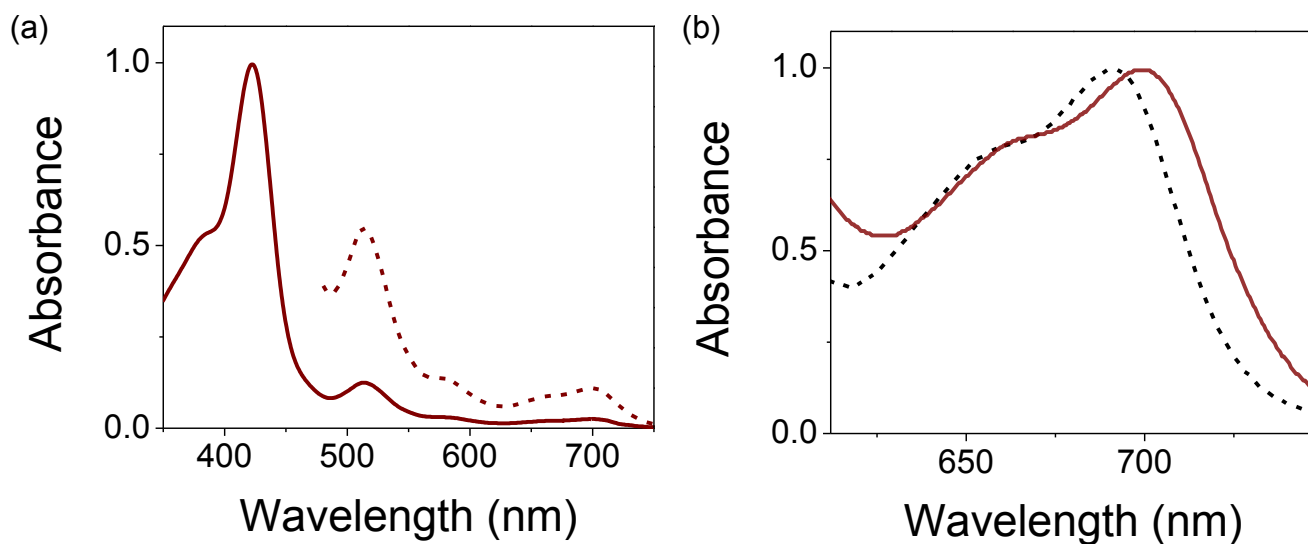
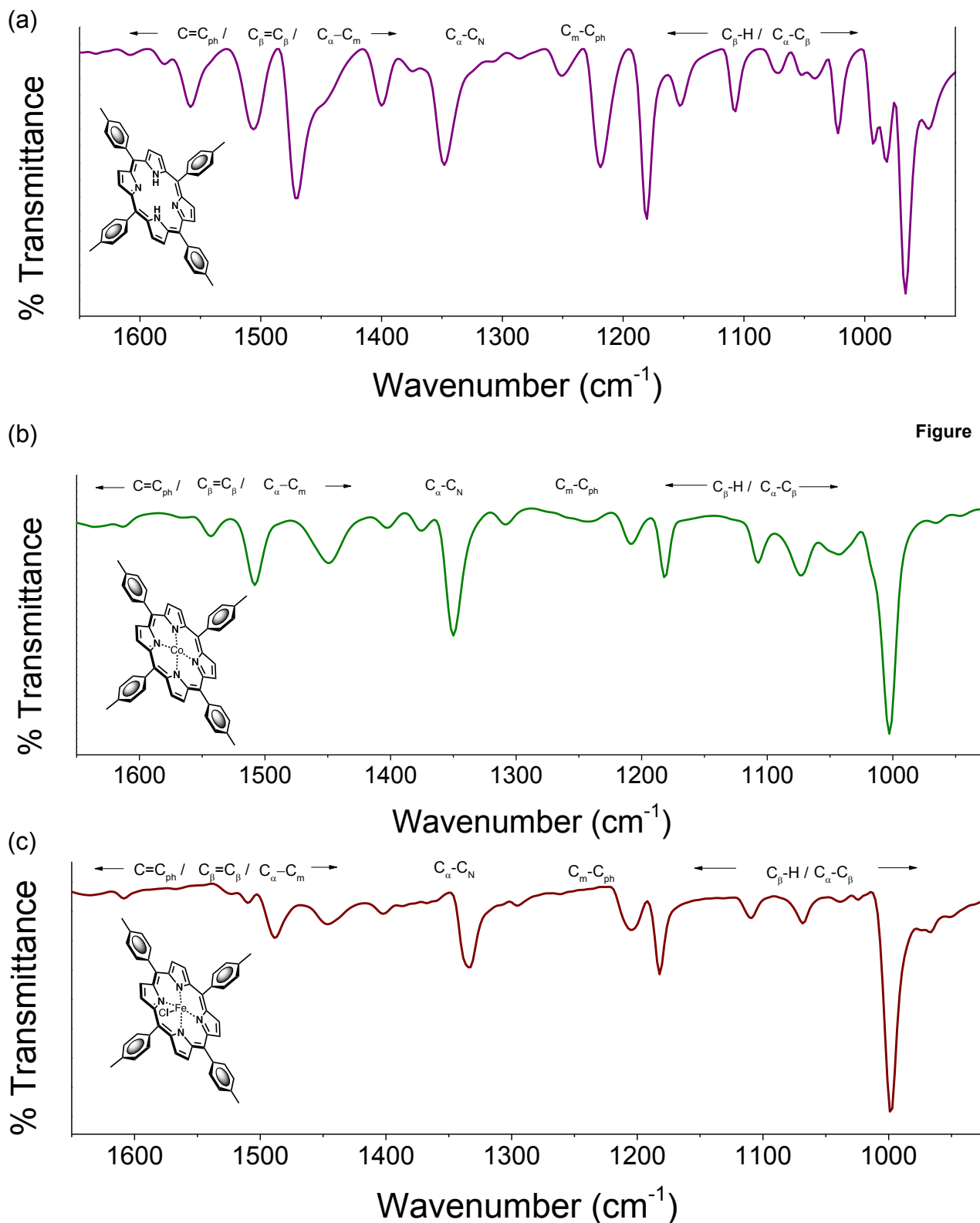


Figure S6. (a) Absorbance spectra of 5,10,15,20-tetra-*p*-tolyl-2-(4-vinylphenyl)porphyrin iron(III) chloride recorded in toluene showing the Soret band normalized to 1 (solid) and the highest energy Q band normalized to 0.5 (dashed). (b) Normalized absorbance spectra showing the lowest energy Q bands of the model compound 5,10,15,20-tetra-*p*-tolylporphyrin iron(III) chloride (dashed) and 5,10,15,20-tetra-*p*-tolyl-2-(4-vinylphenyl)porphyrin iron(III) chloride (solid) are included for comparison.

1.3 FTIR data



FTIR transmission spectra of the model compounds: (a) 5,10,15,20-tetra-*p*-tolylporphyrin, (b) 5,10,15,20-tetra-*p*-tolylporphyrin cobalt(II), and (c) 5,10,15,20-tetra-*p*-tolylporphyrin iron(III) chloride in KBr.

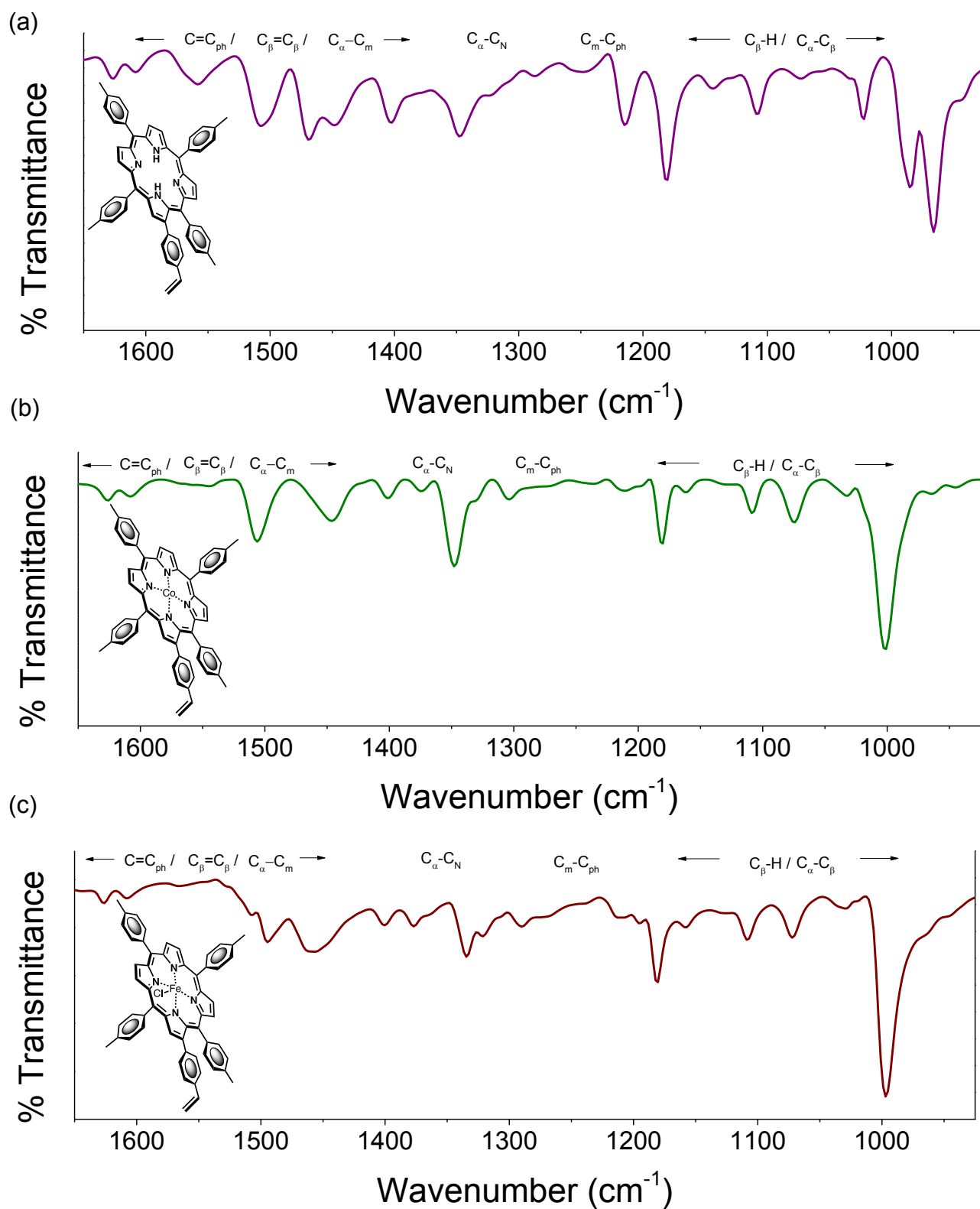


Figure S8. FTIR transmission spectra of the target compounds: (a) 5,10,15,20-tetra-*p*-tolyl-2-(4-vinylphenyl)porphyrin, (b) 5,10,15,20-tetra-*p*-tolyl-2-(4-vinylphenyl)porphyrin cobalt(II), and (c) 5,10,15,20-tetra-*p*-tolyl-2-(4-vinylphenyl)porphyrin iron(III) chloride in KBr.

1.4 Electrochemical data

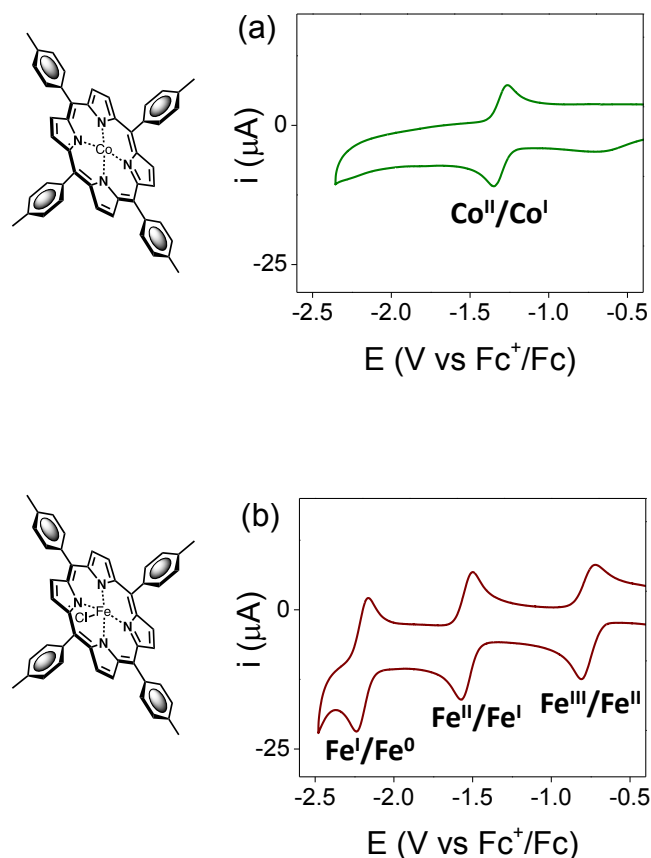


Figure S9. Cyclic voltammograms of (a) 5,10,15,20-tetra-*p*-tolylporphyrin cobalt(II) (CoTTP) and (b) 5,10,15,20-tetra-*p*-tolylporphyrin iron(III) chloride (FeTTP) recorded in 0.1 M tetrabutylammonium hexafluorophosphate in butyronitrile using a glassy carbon working electrode and a scan rate of 250 mV s⁻¹. The counter electrode was a platinum wire and the potential of the silver wire pseudoreference electrode was determined using the ferrocenium/ferrocene (Fc⁺/Fc) redox couple as an internal standard.

Compound	^{III} E	^{II} E	^I E
CoTTP	NA	NA	-1.33 (ΔE _p = 90 mV)
FeTTP	-2.21 (ΔE _p = 80 mV)	-1.56 (ΔE _p = 80 mV)	-0.78 (ΔE _p = 84 mV)

Table S1. Midpoint potentials for the reduction (ⁿE_{1/2}) of 5,10,15,20-tetra-*p*-tolylporphyrin cobalt(II) (CoTTP) and 5,10,15,20-tetra-*p*-tolylporphyrin iron(III) chloride (FeTTP) as determined by cyclic voltammetry and reported in V vs Fc⁺/Fc. Peak-to-peak separations (ΔE_p) are reported in parenthesis. The electrolyte was 0.1 M tetrabutylammonium hexafluorophosphate in butyronitrile and the scan rate was 250 mV s⁻¹. The working electrode was glassy carbon, the counter electrode was a platinum wire, and the potential of the silver wire pseudoreference electrode was determined using the ferrocenium/ferrocene redox couple as an internal standard.

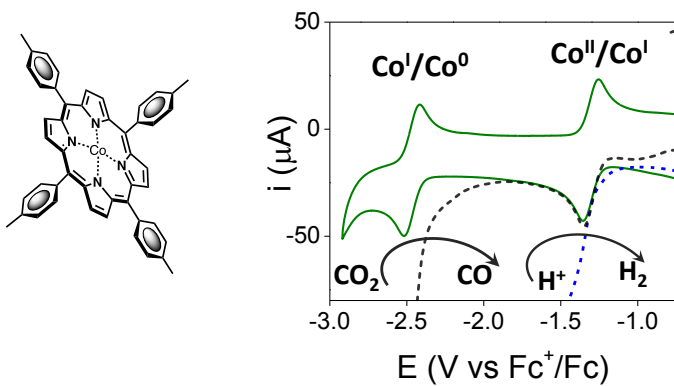


Figure S10. Voltammograms of 5,10,15,20-tetra-*p*-tolylporphyrin cobalt(II) (CoTTP) recorded in 0.1 M tetrabutylammonium hexafluorophosphate in: dimethylformamide under argon (green solid), 10 mM tosic acid in dimethylformamide under argon (blue dash) or dimethylformamide under CO₂ (black dash). All voltammograms were recorded using a glassy carbon working electrode and a scan rate of 250 mV s⁻¹. The counter electrode was a platinum wire and the potential of the silver wire pseudoreference electrode was determined using the ferrocenium/ferrocene (Fc⁺/Fc) redox couple as an internal standard.

2. Surface characterization

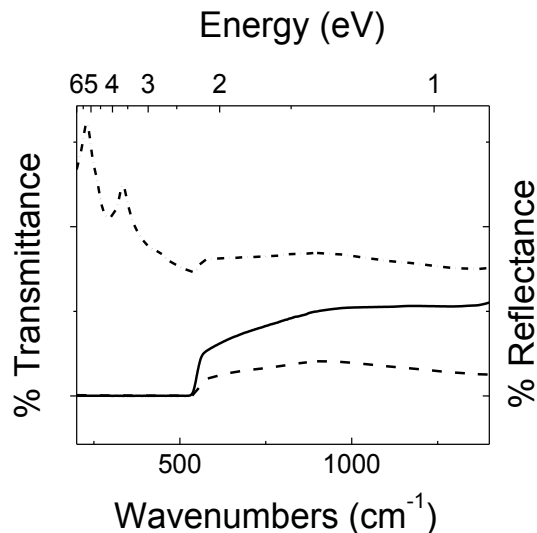


Figure S11. Optical spectra of GaP (100) including: transmission (solid), relative specular reflectance (dash dot), and diffuse reflectance (dash).

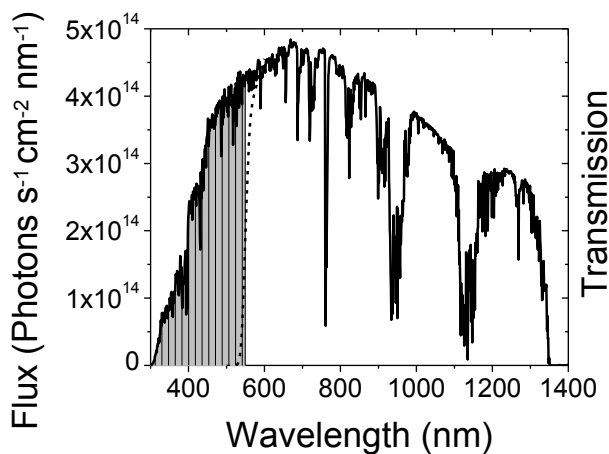


Figure S12. The air mass 1.5 global tilt solar flux spectrum (solid) and the transmission spectrum of the GaP substrates used in these experiments (dash). The shaded grey area shows the integrated region of the solar spectrum from 280 nm up to the band gap of GaP ($E_g = 2.26 \text{ eV} = 549 \text{ nm}$), representing the theoretical maximum number of photons ($6.0 \times 10^{16} \text{ photons s}^{-1} \text{ cm}^{-2}$) that can be collected. If all available photons give rise to current, the maximum theoretical photocurrent density is 9.6 mA cm^{-2} . However, actual photocurrent densities are always lower given reflection and transmission losses as well as other “parasitic” processes that preclude absorbed photons from being converted to charge carriers moving through a potential. In addition, catalysts immobilized on a surface can also absorb a fraction of the incident photons.⁵

2.1 FTIR data

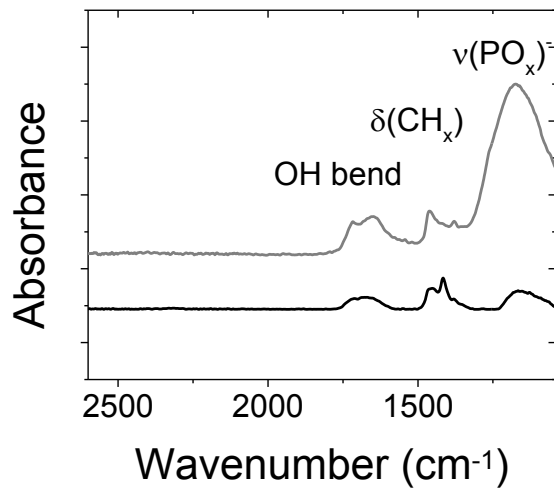


Figure S13. GATR-FTIR absorbance spectra of unmodified GaP(100) before (gray) and after (black) etching with HF.

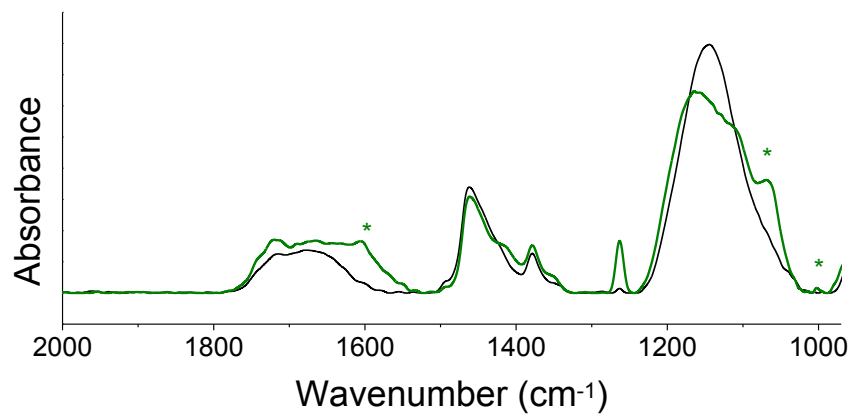


Figure S14. GATR-FTIR absorbance spectra of CoP-GaP (green) and unmodified GaP(100) (black). The porphyrin related absorbance bands observed on the modified-GaP surfaces are consistent with previous literature reports regarding the peak positions of analogous non-surface immobilized porphyrins.^{6,7}

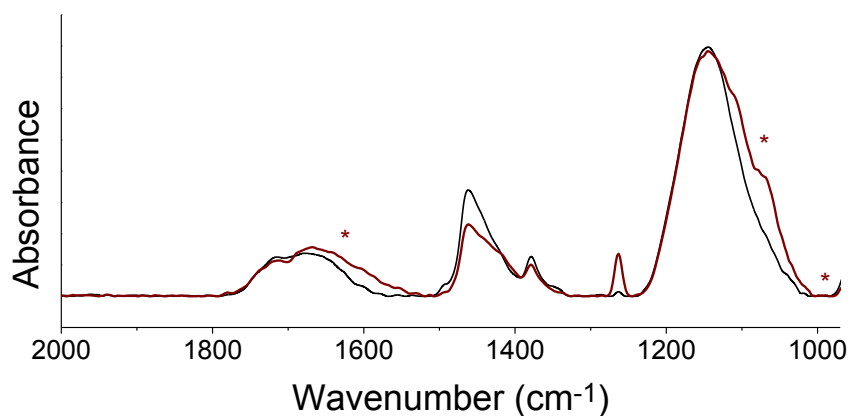


Figure S15. GATR-FTIR absorbance spectra of FeP-GaP (dark red) and unmodified GaP(100) (black). The porphyrin related absorbance bands observed on the modified-GaP surfaces are consistent with previous literature reports regarding the peak positions of analogous non-surface immobilized porphyrins.^{4,7}

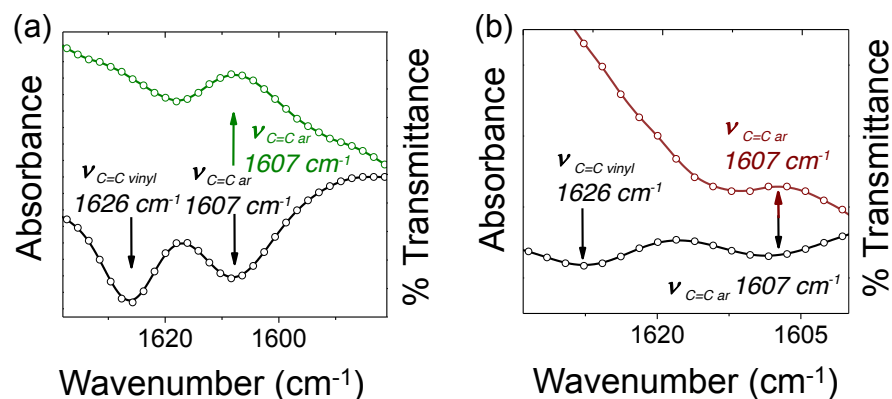


Figure S16. (a) GATR-FTIR absorbance spectra of CoP-GaP (green) and FTIR transmission spectra of the cobalt porphyrin precursor, 5,10,15,20-tetra-*p*-tolyl-2-(4-vinylphenyl)porphyrin cobalt(II) (black). (b) GATR-FTIR absorbance spectra of FeP-GaP (dark red) and FTIR transmission spectra of the iron porphyrin precursor, 5,10,15,20-tetra-*p*-tolyl-2-(4-vinylphenyl)porphyrin iron(III) (black).

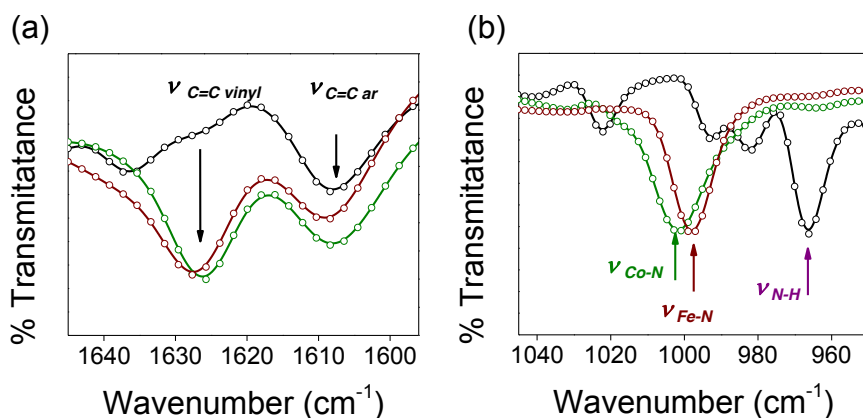


Figure S17. FTIR transmittance spectra 5,10,15,20-tetra-*p*-tolylporphyrin (black), 5,10,15,20-tetra-*p*-tolyl-2-(4-vinylphenyl)porphyrin cobalt(II) (green), and 5,10,15,20-tetra-*p*-tolyl-2-(4-vinylphenyl)porphyrin iron(III) chloride (dark red) in KBr.

2.2 XPS data

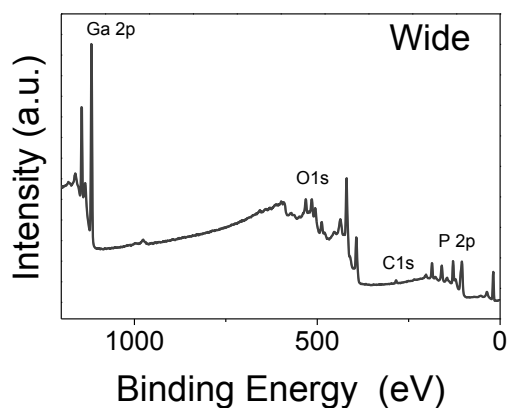


Figure S18. XP survey spectrum of unmodified GaP(100).

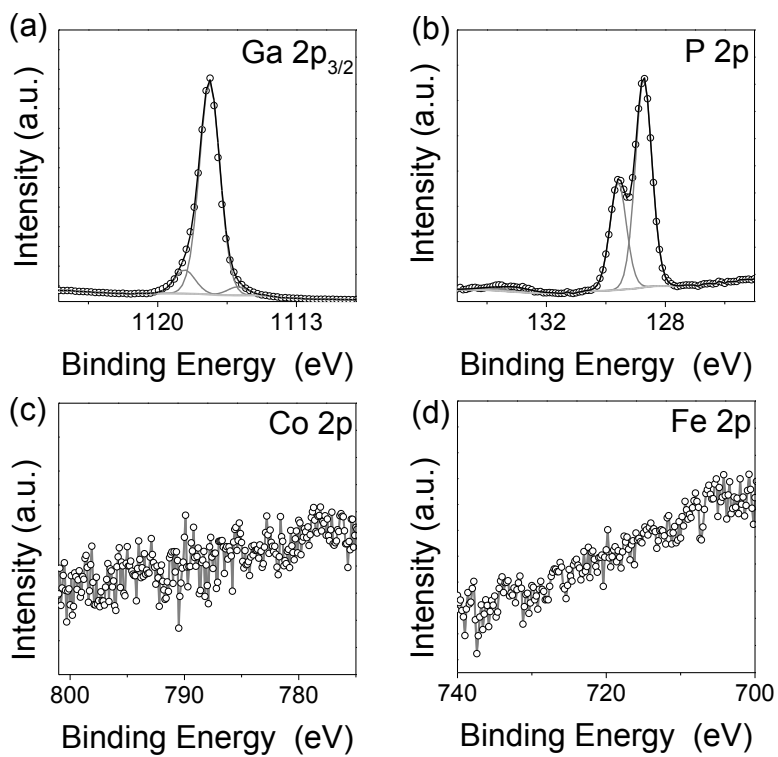


Figure S19. Core level XP spectra of unmodified GaP(100) showing the (a) Ga $2p_{3/2}$, (b) P 2p, (c) Co 2p, and (d) Fe 2p regions. In the Ga $2p_{3/2}$ and P 2p core level spectra (a & b), the circles (gray) are the spectral data, and the solid lines represent the background (light gray), component fit (gray), and overall fit (black).

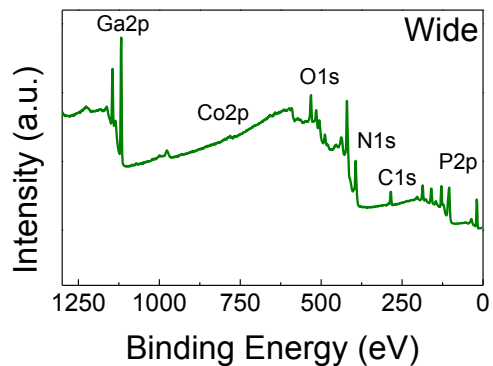


Figure S20. XP survey spectrum of CoP-GaP.

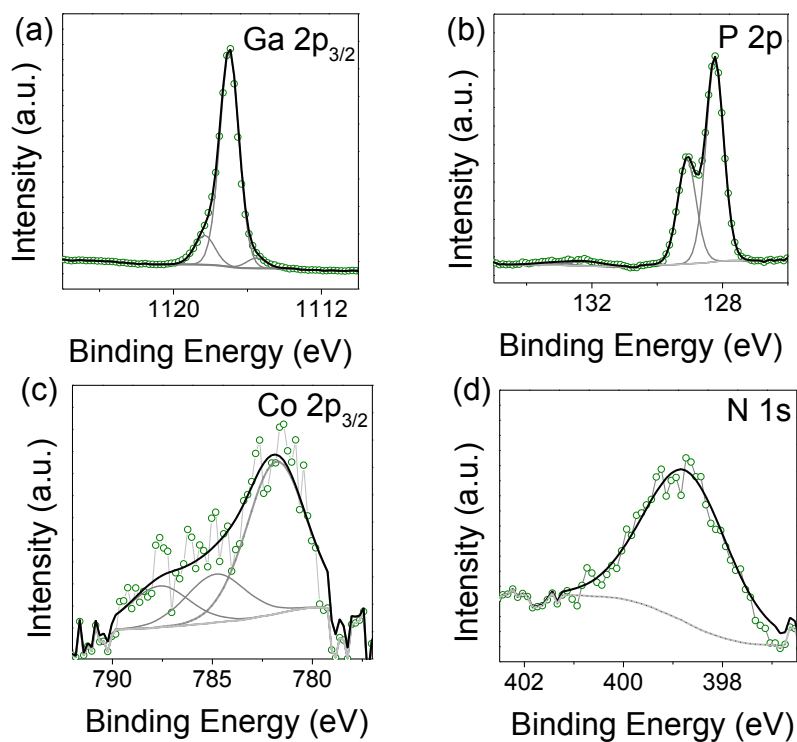


Figure S21. Core level XP spectra of CoP-GaP showing the (a) Ga $2p_{3/2}$, (b) P $2p$, (c) Co $2p_{3/2}$, and (d) N $1s$ regions. In all spectra, the circles (green) are the spectral data, and the solid lines represent the background (light gray), component fit (gray), and overall fit (black). These peak positions are consistent with previous literature reports on XP measurements of cobalt porphyrins.^{8,9}

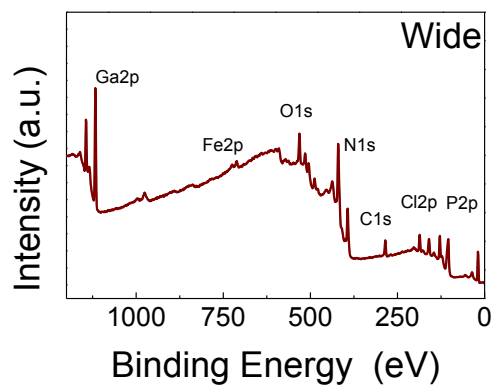


Figure S22. XP survey spectrum of FeP-GaP.

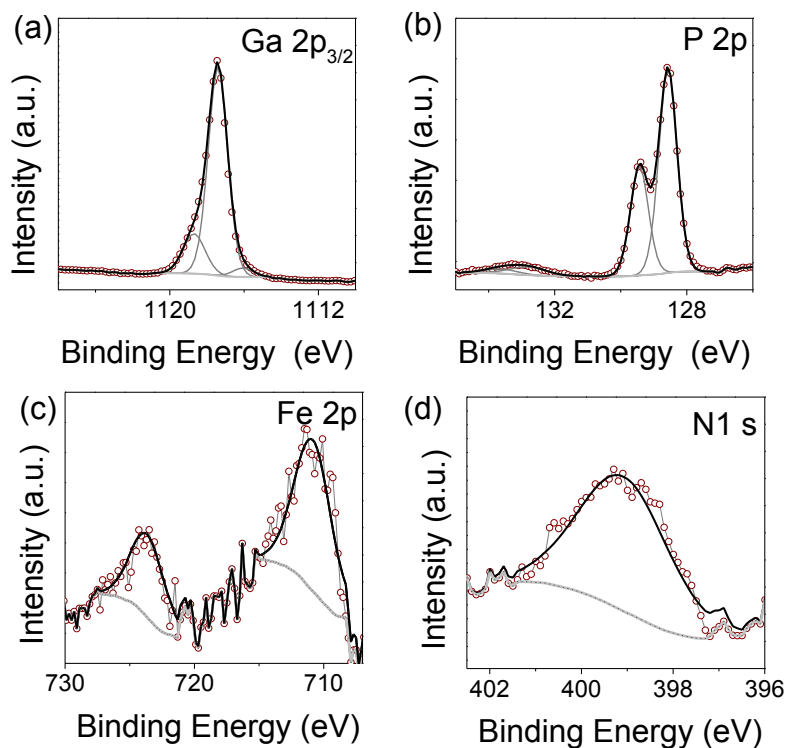


Figure S23. Core level XP spectra of FeP-GaP showing (a) Ga $2p_{3/2}$, (b) P 2p, (c) Fe 2p, and (d) N 1s regions. In all spectra, the circles (dark red) are the spectral data, and the solid lines represent the background (light gray), component fit (gray), and overall fit (black). These peak positions are consistent with previous literature reports on XP measurements of cobalt porphyrins.¹⁰

3. Photoelectrochemical data

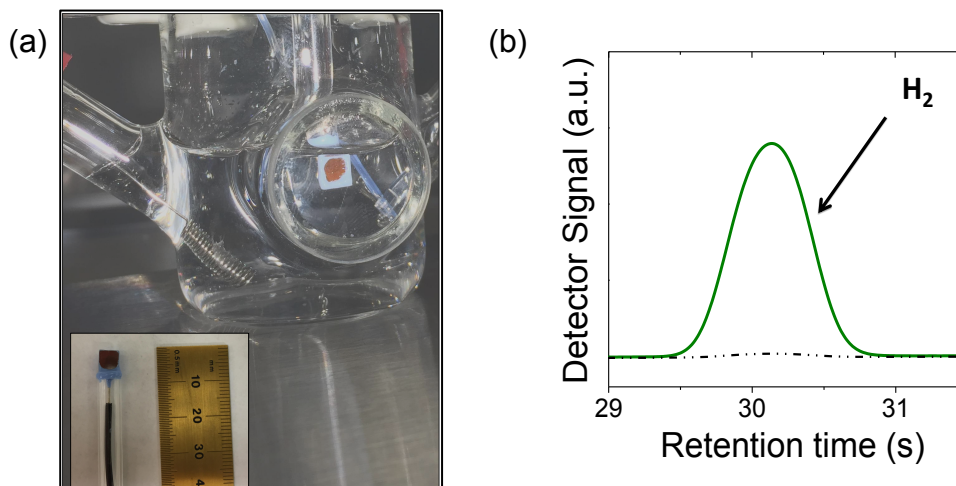


Figure S24. (a) Photo of the photoelectrochemical cell used in this report and equipped with a CoP-GaP photoelectrode (working electrode), platinum coil (counter electrode) and Ag/AgCl electrode (reference electrode) in aqueous conditions (pH 7, 0.1 M phosphate buffer). (b) Gas chromatograms obtained using samples of the headspace gas collected from a sealed photoelectrochemical cell equipped with a CoP-GaP working electrode polarized at 0 V vs RHE. The samples were collected before (dash dot) and after (solid) 30 min of illumination (100 mW cm^{-2}).

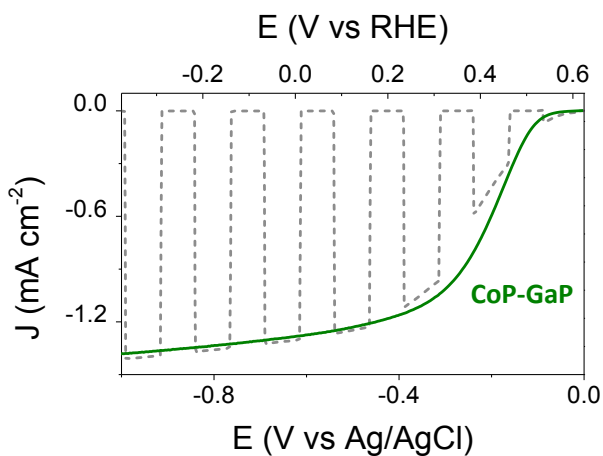


Figure S25. Linear sweep voltammograms recorded using a CoP-GaP working electrode in phosphate buffer (pH 7) under intermittent (gray dash) and constant (green solid) 1-sun illumination at a scan rate of 100 mV s^{-1} .

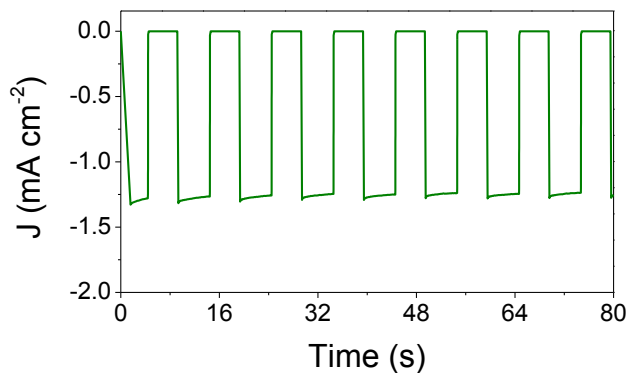


Figure S26. Three-electrode electrolysis measurements using a CoP-GaP working electrode polarized at 0 V vs RHE in phosphate buffer (pH 7) under intermittent 1-sun illumination.

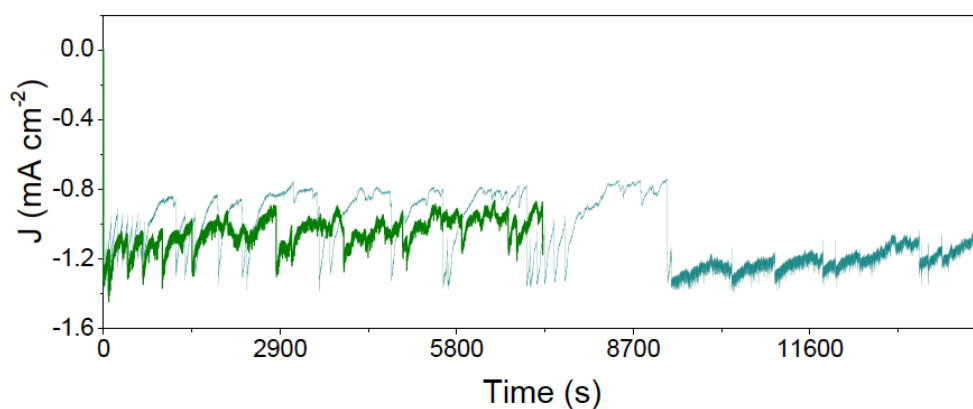


Figure S27. Three-electrode electrolysis measurements using CoP-GaP working electrodes polarized at 0 V vs RHE in phosphate buffer (pH 7) under 1-sun illumination for 2 h (green) and 4 h (teal). The current density (J) represents the amount of current generated per unit cross-sectional area of the CoP-GaP working electrodes (not the electrolyte exposed surface area). During these measurements, hydrogen gas bubbles accumulating on the surface of the working electrodes are periodically dislodged from the sample, resulting in the sudden change in current density due to a sudden change in the electrolyte exposed surface area.

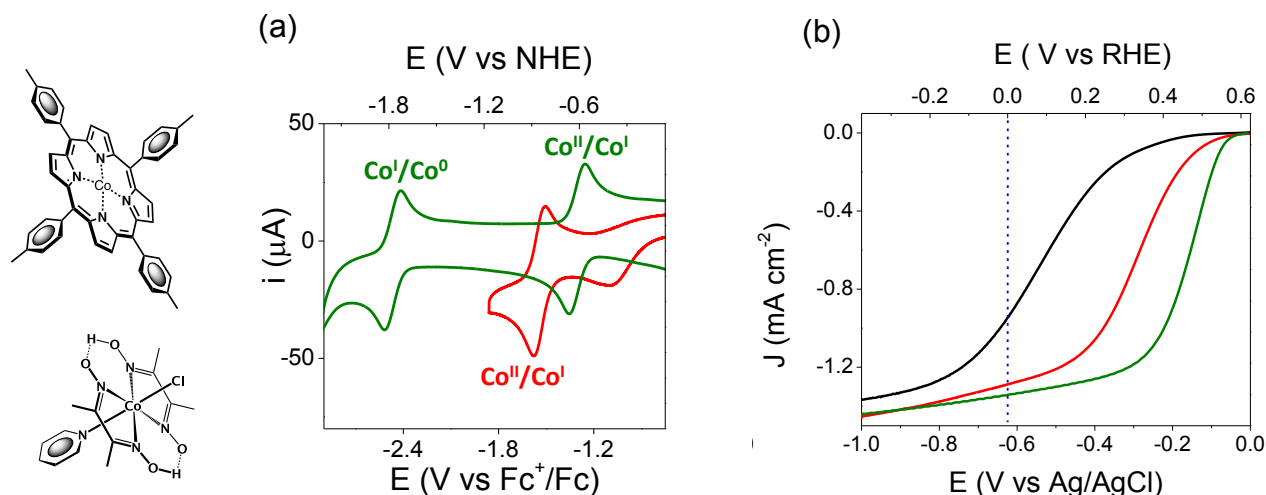


Figure S28. (a) Cyclic voltammograms of 5,10,15,20-tetra-*p*-tolylporphyrin cobalt(II) (CoTTP) (green) and a model cobaloxime complex, Co(dmgh)₂(Py)Cl, (red) recorded in 0.1 M tetrabutylammonium hexafluorophosphate in dimethylformamide using a glassy carbon working electrode and a scan rate of 250 mV s⁻¹. As recommended by IUPAC¹², electrode potentials in nonaqueous solvents are reported with respect to the ferrocenium/ferrocene redox couple (V vs Fc⁺/Fc) as a reference redox system. Conversion to a normal hydrogen electrode scale (V vs NHE) is included to facilitate comparisons (with E_{1/2} of the Fc⁺/Fc couple taken as 0.45 V vs. SCE¹³ and the potential of the SCE electrode taken as 0.241 V vs NHE¹⁴). This latter method of reporting potentials is not recommended in large part because it involves conversion from actual experimentally measured potentials to potentials versus a theoretical reference standard.¹⁵ (b) Linear sweep voltammograms recorded using CoP-GaP (green), cobaloxime-polyvinylpyridine-GaP¹¹ (red), or unmodified GaP(100) (black) working electrodes in phosphate buffer (pH 7) at a scan rate, 100 mV s⁻¹ under 100 mW cm⁻² illumination. The dashed line at 0 V vs RHE represents the reversible hydrogen electrode potential (-0.41 V vs NHE at pH 7).

Compound	^{III} E	^{II} E	^I E
CoTTP	NA	-2.47 (ΔE _p = 100 mV)	-1.3 (ΔE _p = 100 mV)
Co(dmgh) ₂ (Py)Cl	NA	NA	-1.55 (ΔE _p = 70 mV)

Table S2. Midpoint potentials for the reduction (ⁿE_{1/2}) of 5,10,15,20-tetra-*p*-tolylporphyrin cobalt(II) (CoTTP) and a model cobaloxime complex, Co(dmgh)₂(Py)Cl, as determined by cyclic voltammetry and reported in V vs Fc⁺/Fc. Peak-to-peak separations (ΔE_p) are reported in parenthesis. The electrolyte was 0.1 M tetrabutylammonium hexafluorophosphate in dimethylformamide, and the scan rate was 250 mV s⁻¹. The working electrode was glassy carbon, the counter electrode was a platinum wire, and the potential of the silver wire pseudoreference electrode was determined using the ferrocenium/ferrocene redox couple as an internal standard.

3.1 Spectral profile of a LSC-100 Series Oriel Solar Simulator

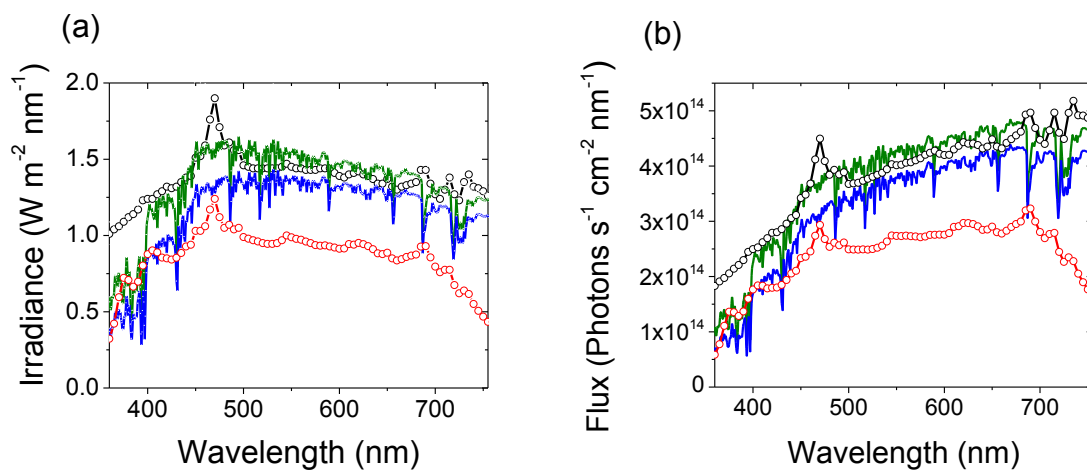


Figure S29. (a) Spectral Irradiance and (b) photon flux of a LSC-100 Series Oriel Solar Simulator collected with (red circles) and without (black circles) an AM1.5 filter. For comparison, the air mass 1.5 global tilt (green) and direct circumsolar (blue) spectra are included.¹⁶

4. Supplemental information references

1. Lee, C.H.; Lindsey, J.S. One-Flask Synthesis of *Meso*-Substituted Dipyrromethanes Their Application in the Synthesis of *Trans*-Substituted Porphyrin Building Blocks. *Tetrahedron* **1994**,50(39): 11427-11440.
2. Gao, G.Y.; Ruppel, J.V.; Allen, D.B.; Chen, Y.; Zhang, X.P. Synthesis of β -Functionalized Porphyrins via Palladium-Catalyzed Carbon - Heteroatom Bond Formations: Expedient Entry into β -Chiral Porphyrins. *JOC Artic.* **2007**,72(6): 9060-9066.
3. Chizhova N.V.; Kumeev R.S.; Mamardashvili N.Zh. Synthesis and Spectral Properties of Cobalt (II) and Cobalt (III) Tetraarylporphyrinates. *Russ. J. Inorg. Chem.* **2013**,58(6): 740-743.
4. Sun, Z.-C.; She, Y.-B.; Zhou, Y.; Song X.-F.; Li, Kai. Synthesis, Characterization and Spectral Properties of Substituted Tetraphenylporphyrin Iron Chloride Complexes. *Molecules* **2011**,16: 2960-2970.
5. Trotochaud, L.; Mills, T. J.; Boettcher, S. W.; An Optocatalytic Model for Semiconductor-Catalyst Water-splitting Photoelectrodes Based on In Situ Optical Measurements on Operational Catalyst. *J. Phys. Chem. Lett.* **2013**,4: 931-935.
6. Lu, X.; Geng, Z.; Wang, Y.; Lv, B.; Kang, J. Synthesis and Characterization of Three New Unsymmetrical Porphyrins and Their Cobalt Complexes. *Synth.React. Inorg. Met. Org. Chem.* **2002**,32: 843-851.
7. Costa, A.A.; Ghesti, G.F.; Macedo, J.L.; Braga V.S.; Santos, M.M., Dias, J.A., Dias, S.L. Immobilization of Fe, Mn and Co Tetraphenylporphyrin Complexes in MCM-41 and their Catalytic Activity in Cyclohexene Oxidation Reaction by Hydrogen Peroxide. *J. of Mol. Cat. A* **2008**,282: 149-157.
8. Karweik, D.H.; Winograd, N. Nitrogen Charge Distributions in Free-Base Porphyrins, Metalloporphyrins, and Their Reduced Analogues Observed by X-Ray Photoelectron Spectroscopy. *Inorg. Chem.* **1976**,15: 2336-2342.
9. Flechtner, K.; Andreas Kretschmann, A.; Steinrück, H.-P.; Gottfried, J.M. NO-Induced Reversible Switching of the Electronic Interaction between a Porphyrin-Coordinated Cobalt Ion and Silver Surface. *J. Am. Chem. Soc.* **2007**,129: 12110-12111.
10. Lipińska, M.E.; Novais, J.P.; Rebelo, S.L.-H.; Bachiller-Baeza, B.; Rodriguez-Ramos, I.; Guerrero-Ruiz, A.; Freire, C. Microwave assisted Silylation of Graphite Oxide and Iron (III) Porphyrin Interaction. *Polyhedron* **2014**,81: 475-484.
11. Beiler, A.M.; Khusnutdinova D.; Jacob S.I.; Moore G.F. Chemistry at the interface: Polymer-Functionalized GaP Semiconductors for Solar Hydrogen Production. *Ind. Eng. Chem. Res.* **2016**, 55: 5306-5314.
12. Gritzner, G.; Kuta. Recommendations on reporting electrode potentials in nonaqueous solvents. *J. Pure Appl. Chem.* **1984**, 56: 461-466.
13. Connelly, N. G.; Geiger, W. E. Chemical Redox Agents for Organometallic Chemistry. *Chem. Rev.* **1996**, 96, 877-910.
14. Bard, A. J.; Faulkner, L. R. *Electrochemical Methods: Fundamentals and Applications*, 2nd edn. Wiley & Sons: New York, 2001.
15. Kadish, K. M.; Smith, K. M.; Guillard, R. *The Porphyrin Handbook: Electron transfer*, Volume 8, 2000
16. At the time of writing, the air-mass 1.5 global tilt (AM 1.5G) and direct circumsolar (AM 1.5D) solar spectra, from the ASTM G173-03 data set, is available online at <http://rredc.nrel.gov/solar/spectra/am1.5/>.